The TRAPUM large magellanic cloud pulsar survey with MeerKAT I: survey set-up and first seven pulsar discoveries

V. Prayag [1,2]★ L. Levin,[3] M. Geyer [1,2] B. W. Stappers [3] E. Carli,[3] E. D. Barr,[4] R. P. Breton [3] S. Buchner,[5] M. Burgay [6] M. Kramer,[4] A. Possenti,[6] V. Venkatraman Krishnan,[4] C. Venter [7,8] J. Behrend,[4] W. Chen [4] D. M. Horn,[5] P. V. Padmanabh[4,9,10] and A. Ridolfi [4,6]

[1] *Department of Astronomy, The University of Cape Town, Private Bag X3, Rondebosch 7701 Cape Town, South Africa*
[2] *High Energy Physics, Cosmology & Astrophysics Theory (HEPCAT) Group, Department of Mathematics & Applied Mathematics, University of Cape Town, 7700 Cape Town, South Africa*
[3] *Jodrell Bank Centre for Astrophysics, Department of Physics and Astronomy, The University of Manchester, M13 9PL Manchester, United Kingdom*
[4] *Max-Planck-Institut für Radioastronomie, Auf Hügel 69, D-53121 Bonn, Germany*
[5] *South African Radio Astronomy Observatory (SARAO), 2 Fir Street, Black River Park, Observatory, 7925 Cape Town*
[6] *INAF-Osservatorio Astronomico di Cagliari, via della Scienza 5, 09047 Selargius (CA), Italy*
[7] *Centre for Space Research, North-West University, Private Bag X6001, 2520 Potchefstroom, South Africa*
[8] *National Institute for Theoretical and Computational Sciences (NITheCS), Stellenbosch, 7604, South Africa*
[9] *Max-Planck-Institut für Gravitationsphysik (Albert-Einstein-Institut), D-30167 Hannover, Germany*
[10] *Leibniz Universität Hannover, D-30167 Hannover, Germany*

ABSTRACT

The Large Magellanic Cloud (LMC) presents a unique environment for pulsar population studies due to its distinct star formation characteristics and proximity to the Milky Way. As part of the TRAPUM (TRAnsients and PUlsars with MeerKAT) Large Survey Project, we are using the core array of the MeerKAT radio telescope (MeerKAT) to conduct a targeted search of the LMC for radio pulsars at *L*-band frequencies, 856–1712 MHz. The excellent sensitivity of MeerKAT, coupled with a 2-h integration time, makes the survey 3 times more sensitive than previous LMC radio pulsar surveys. We report the results from the initial four survey pointings which have resulted in the discovery of seven new radio pulsars, increasing the LMC radio pulsar population by 30 per cent. The pulse periods of these new pulsars range from 278 to 1690 ms, and the highest dispersion measure is $254.20 \, \mathrm{pc \, cm^{-3}}$. We searched for, but did not find any significant pulsed radio emission in a beam centred on the SN 1987A remnant, establishing an upper limit of $6.3 \, \mu\mathrm{Jy}$ on its minimum flux density at 1400 MHz.

Key words: pulsars: general – pulsars: individual: PSR J0509−6838, PSR J0509−6845, PSR J0518−6939, PSR J0518−6946, PSR J0519−6931, PSR J0534−6905 – galaxies: individual: Large Magellanic Cloud – Magellanic Clouds.

1 INTRODUCTION

The Large Magellanic Cloud (LMC) and the Small Magellanic Cloud (SMC) are two irregular galaxies and the closest galactic companions to the Milky Way. As a result, the Magellanic Clouds have been an enduring reference for drawing parallels and contrasts with our Galaxy. They offer an ideal setting for the study of stellar populations and how their environments impact the process of star formation. Situated beyond the boundaries of the disc of the Milky Way at a distance of 49.6 kpc (Graczyk et al. 2020), the LMC benefits from a particularly advantageous observational angle, notably from the Southern Hemisphere, with a lower line-of-sight dust extinction in comparison to our own Galaxy.

The SMC has a low-average metallicity of $[Fe/H] = (−0.97 \pm 0.05)$ dex (Choudhury et al. 2020), implying that it will have a distinct stellar environment with less massive stars being formed (Pakmor et al. 2022). In contrast, the LMC has a similar mean stellar metallicity, $[Fe/H] = (−0.42 \pm 0.04)$ dex (Choudhury et al. 2021), to that of the thin disc of the Milky Way, $[Fe/H] = −0.5$ dex (Matteucci 2014), which allows us to compare the star formation histories between the two galaxies. The LMC has a greater abundance of supernova remnants (SNRs, Badenes, Maoz & Draine 2010; Zangrandi et al. 2024) and high-mass X-ray binaries (HMXBs; Liu, van Paradijs & van den Heuvel 2005; Antoniou & Zezas 2016) per unit mass than our Galaxy, giving an indication of the high star formation rate prevailing there (Grimm, Gilfanov & Sunyaev 2003). Consequently, it is anticipated that a larger proportionate population of isolated young neutron stars (hereafter, NSs) and NSs in binary systems, especially with massive star companions, will be found within the LMC. Young pulsars, generally rotation-powered, are often associated with SNRs, and they tend to have irregular rotation patterns which are attributed to 'glitches' and timing noise (e.g. Lyne 1999; Haskell & Melatos 2015; Basu et al. 2022). Accretion-powered

★ E-mail: venu_prayag@hotmail.com

pulsars, such as the progenitors to millisecond pulsars (MSPs), are found in binaries. The transfer of angular momentum during the accretion phase of binaries leads to MSPs having pulse periods typically shorter than 10 ms (Alpar et al. 1982; Radhakrishnan & Srinivasan 1982; Papitto et al. 2013).

The present pulsar population of the LMC consists of 25 pulsars, while the SMC is home to 16 pulsars (Manchester et al. 2005).[1] Out of these, 14 from the SMC (see Carli et al. 2024) and 24 from the LMC have been detected in the radio domain. Together, these 38 pulsars constitute the extragalactic rotation-powered radio pulsar population, which accounts for only about 1 per cent of the more than 3500 radio pulsars discovered to date.

Currently, there is only one known extragalactic binary pulsar system, PSR J0045−7319, located in the SMC (McConnell et al. 1991; Kaspi et al. 1994). The potential discovery of binary systems in the LMC, particularly double NS systems, could provide valuable insights into the extragalactic NS population and the rate of extragalactic NS mergers. In addition, recent evidence for the gravitational wave background using pulsar timing arrays (Agazie et al. 2023; EPTA Collaboration 2023; Reardon et al. 2023; Xu et al. 2023) highlights the significance of discovering stable extragalactic MSPs. Pulsars located closely together in the sky exhibit a significantly greater timing correlation due to the gravitational wave Earth-term, compared to pulsars with greater spatial separations. So far, there have been no MSPs found in the Magellanic Clouds.

Pulsars within the LMC provide a unique line-of-sight that passes through the interstellar medium (ISM) of the LMC and that of the Milky Way, as well as the intergalactic medium. As pulsar signals propagate through these regions, they interact with electrons, causing dispersion that follows a quadratic dependence on radio frequency. This is quantified as the dispersion measure (DM), which depends on the total electron column density between Earth and the pulsar. By finding a large number of radio pulsars in different locations of the LMC, we can probe the different regions, enhancing our understanding of their electron density content.

One telescope which has the required sensitivity and optimal geographical location to efficiently observe the LMC is the Parkes 64 m radio telescope, recently given the indigenous Wiradjuri name 'Murriyang' (hereafter, Murriyang), located in New South Wales, Australia. Murriyang has played, and continues to play, an instrumental role in the search for pulsars, having discovered 22 out of the 25 known pulsars in the LMC (McCulloch et al. 1983; McConnell et al. 1991; Crawford et al. 2001; Manchester et al. 2006; Ridley et al. 2013; Hisano et al. 2022).

MeerKAT (Jonas & MeerKAT Team 2016; Camilo et al. 2018), located in the Karoo in the Northern Cape province of South Africa at a latitude of −30°43′ (Bailes et al. 2020), is a state-of-the-art radio telescope also well placed to observe the LMC. Transients and Pulsars with MeerKAT.[2] (TRAPUM) is a large survey project with the aim to search for new pulsars, as well as various transient phenomena at radio frequencies (Stappers & Kramer 2016). One of the objectives of TRAPUM is to survey the Magellanic Clouds and here, we report the results from the first four pointings of the TRAPUM LMC Survey.

Our paper is structured as follows: in Section 2, we review previous surveys of the LMC and examine the current LMC pulsar population. We describe our approach to source selection and the planning of observations in Section 3. In Section 4, we outline the observation set-up and the search process. We present the results obtained from the initial four pointings of the survey in Section 5. Finally, in Section 6, we conclude on our findings.

2 PREVIOUS SURVEYS AND DISCOVERIES

The first discovery of a pulsar in the LMC, PSR J0529−6652, and in fact, the first extragalactic radio pulsar discovery, was made by McCulloch et al. (1983). The discovery was part of a survey of the Magellanic Clouds using Murriyang, undertaken between 1980 and 1987, that was eventually improved and extended by McConnell et al. (1991), yielding two more pulsars in the LMC. The observations lasted 5000 s each, with the most common observation parameters being a centre frequency of 610 MHz and a total bandwidth of 60 MHz spread across 24 channels. The implementation of the Murriyang multibeam receiver (Staveley-Smith et al. 1996) paved the way for higher sensitivity surveys such as the Parkes Multibeam Pulsar Survey (PMPS), which focused on the Galactic plane (Manchester et al. 2001), conducted between 2000 and 2001. Around the same time, using the Murriyang multibeam receiver, Manchester et al. (2006) searched for radio pulsars in the Magellanic Clouds. The most recent, and still ongoing, LMC survey using Murriyang, initiated in the year 2009, is known as the High-Resolution LMC Survey (Ridley et al. 2013; Hisano et al. 2022).

Manchester et al. (2006) observed the LMC using a total of 136 pointings, amounting to 1768 beams. Each pointing was observed for a duration of 8400 s, with a sampling time of 1000 μs, a centre frequency of 1374 MHz, and a bandwidth of 288 MHz spread across 96 channels. The High Resolution LMC Survey kept the same centre frequency and improved on its predecessor by increasing the length of observation, the bandwidth, and the number of channels to 8600 s, 340 MHz, and 1024 channels, respectively. The sampling time was also reduced to 64 μs following the installation of the Berkeley Parkes Swinburne Recorder (BPSR; Keith et al. 2010).

A total of 13 pulsars were discovered in the LMC from the PMPS by Manchester et al. (2006), with five found from a reprocessing of the data later on by Ridley et al. (2013). With 54 out of 136 pointings completed, the High Resolution LMC survey has yielded four new radio pulsars so far (Ridley et al. 2013; Hisano et al. 2022).

The 'Crab twin' pulsar, PSR J0540−6919 (Seward, Harnden & Helfand 1984), and PSR J0537−6910 (Marshall et al. 1998) were discovered in X-ray observations. PSR J0540−6919 was subsequently observed across various wavelengths, including optical (Middleditch & Pennypacker 1985), radio (Manchester et al. 1993a), and in gamma rays (Marshall et al. 2016), while PSR J0537−6910 remains exclusively detectable at X-rays. Interestingly, Crawford et al. (2001) made the serendipitous discovery of PSR J0535−6935 while trying to observe radio signals from PSR J0537−6910. The detection of PSR J0535−6935 was in observation data of lengths 21600 and 17200 s. The only currently known radio pulsar in the LMC for which radio pulsations have not been discovered by Murriyang is PSR J0523−7125, found in the Australian Square Kilometre Array Pathfinder (ASKAP) Variables and Slow Transients survey (Wang et al. 2022), with both MeerKAT and Murriyang used afterwards to confirm the discovery. Table 1 shows the properties of the known LMC pulsar population.

3 SOURCE SELECTION

To optimize our search strategies, we compiled an extensive list of known sources in the LMC that are likely to harbour pulsars. These included SNRs and candidate SNRs (Bozzetto et al. 2017;

Table 1. Table adapted from Ridley et al. (2013) showing the list of the 25 known LMC rotation-powered pulsars along with their spin periods, P, their fluxes at 1400 MHz, $S_{1400\,MHz}$, their dispersion measures, DM, and their respective discovery papers (Manchester et al. 2005). The $S_{1400\,MHz}$ values, which are not necessarily discovery flux densities, were obtained from Ridley et al. (2013), Xie et al. (2019), Wang et al. (2022), Hisano et al. (2022), and Johnston et al. (2022). The flux densities for eight pulsars are quoted as lower limits as these are not well localized, as reported in Ridley et al. (2013). PSR J0537−6910 is known to solely emit X-ray pulsations.

Pulsar JName	P (ms)	$S_{1400\,MHz}$ (μJy)	DM (pc cm^{-3})	Discovery paper
J0449−7031	479.16	56	65.83	Manchester et al. (2006)
J0451−67	245.45	50	45	Manchester et al. (2006)
J0455−6951	320.42	83	94.70	McConnell et al. (1991)
J0456−69	117.07	>150	103	Ridley et al. (2013)
J0456−7031	800.13	13	100.3	Manchester et al. (2006)
J0457−69	231.39	>50	91	Ridley et al. (2013)
J0458−67	1133.9	>70	97	Ridley et al. (2013)
J0502−6617	691.25	250	68.9	McConnell et al. (1991)
J0519−6932	263.21	130	118.86	Manchester et al. (2006)
J0521−68	433.42	>120	136	Ridley et al. (2013)
J0522−6847	674.53	83	126.45	Manchester et al. (2006)
J0523−7125	322.50	1000	157.5	Wang et al. (2022)
J0529−6652	975.74	213	103.31	McCulloch et al. (1983)
J0532−6639	642.74	42	69.2	Manchester et al. (2006)
J0532−69	1149.2	>50	124	Ridley et al. (2013)
J0534−6703	1817.6	116	95.3	Manchester et al. (2006)
J0535−66	210.52	>30	75	Ridley et al. (2013)
J0535−6935	200.51	50	93.7	Crawford et al. (2001)
J0537−69	112.61	>40	273	Ridley et al. (2013)
J0537−6910	16.122	–	–	Marshall et al. (1998)
J0540−6919	50.570	100	147.2	Seward et al. (1984)
J0542−68	425.19	>140	114	Ridley et al. (2013)
J0543−6851	708.95	87	134.9	Manchester et al. (2006)
J0555−7056	827.84	58	72.9	Manchester et al. (2006)
J0556−67	790.55	120	71	Hisano et al. (2022)

Maitra et al. 2019, 2021; Yew et al. 2021; Kavanagh et al. 2022; Sasaki et al. 2022; Bozzetto et al. 2023; Zangrandi et al. 2024), HMXBs (Antoniou & Zezas 2016; Maitra et al. 2019, 2021; Haberl et al. 2022), globular clusters (GCs, The SIMBAD astronomical data base[3]; Wenger et al. 2000), and pulsar wind nebulae (PWNe; Manchester, Staveley-Smith & Kesteven 1993b; Gotthelf & Wang 2000; Wang et al. 2001; Gaensler et al. 2003; Williams et al. 2005; Bamba et al. 2006; Haberl et al. 2012). Below, we describe the motivation behind each of these types of astrophysical targets.

3.1 Supernova remnants and candidate supernova remnants

Given that NSs originate from the aftermath of massive stars going supernova (Baade & Zwicky 1934), it is intuitive to seek out pulsars within SNRs. Pulsars associated with SNRs are typically young, with examples such as the Crab pulsar and PSR J0540−6919 which are known to emit giant pulses (Johnston & Romani 2003; Geyer et al. 2021). There are more than 60 pulsars that are associated with a SNR (Manchester et al. 2005). These remnants are distinguished by specific characteristics, including a non-thermal power-law radio spectral index steeper than −0.4, diffuse X-ray emissions, and a $[Sii]/H\alpha$ ratio equal to or greater than 0.4. Often, if a source has just one of these features, it is categorized as a candidate SNR

(Bozzetto et al. 2023). The LMC hosts more than 80 SNRs and 40 candidate SNRs (Zangrandi et al. 2024) and to improve our chances of discovering pulsars, we chose to target some of these.

One of these LMC SNRs is arguably the most famous recent supernova that we know of, SN 1987A, a type II supernova located on the fringe of the most energetic star-forming region in the Local Group, 30 Doradus (De Marchi et al. 2011; Fahrion & De Marchi 2024). Since the first detection of neutrinos emanating from SN 1987A (Bionta et al. 1987; Burrows & Lattimer 1987; Hirata et al. 1987), and despite decades of multiwavelength searches (e.g. Manchester & Peterson 1996; Marshall et al. 1998; Alp et al. 2018; Zhang et al. 2018), the existence of a pulsar in the SNR remains to be proven. Zanardo et al. (2018) found some indications for the existence of a compact object when analysing polarization data, while other studies have detected signs of a PWN in the SN 1987A remnant in both radio (Cigan et al. 2019), using the Atacama Large Millimeter/submillimeter Array (ALMA), and X-ray frequencies, using the *Chandra*, *NuSTAR*, and *XMM–Newton* telescopes (Greco et al. 2022). The JWST (JWST; Gardner et al. 2006) provided further insight, peeking through the dust and gas clouds of the SNR at infrared wavelengths, with Fransson et al. (2024) finding emission lines from highly ionized argon and sulphur which they attributed to being produced by a NS. Regarding pulsed radio emission from the SN 1987A remnant, the current best limit is from Zhang et al. (2018), who derived an upper limit of 31 μJy at 1400 MHz by using Murriyang and making use of a signal-to-noise ratio (S/N) threshold of 8. We find that the sky temperature was not taken into account for this upper limit value. If we do include the sky temperature in the direction of the LMC in our calculation, which is 4.0 K at the frequency of 1400 MHz according to the Global Sky Model (Zheng et al. 2017) as in the PYTHON package PYGDSM[4] (Price 2016), we expect an upper limit of 37.2 μJy. Motivated by both this upper limit and our survey sensitivity (see Section 4.2), we chose to conduct a fresh search for a radio pulsar in the SN 1987A remnant using MeerKAT.

3.2 High-mass X-ray binaries

A NS can be recycled through the accretion of matter via Roche lobe overflow in the case of a low-mass X-ray binary (LMXB), or through stellar winds from a companion star in the case of a HMXB, resulting in X-ray emission during what is known as the X-ray binary phase. In a LMXB comprised of a NS and a low-mass companion, material is drawn from the companion star and the NS can be spun-up into the millisecond spin period regime (Alpar et al. 1982; Radhakrishnan & Srinivasan 1982; Tauris & van den Heuvel 2006; Papitto et al. 2013). Accretion processes are expected to alter magnetic field structures, or suppress the emission mechanism responsible for generating radio emission in NSs. Consequently, radio pulsations are generally not expected at this evolutionary stage (Fornasini, Antoniou & Dubus 2023; van den Eijnden & Rajwade 2024). Most pulsars found in HMXBs are exclusively X-ray pulsars, and over 80 of them have been discovered in the Milky Way (Kim, Izmailova & Aimuratov 2023). A few radio pulsars have been discovered in systems believed to have evolved from HMXBs (e.g. Johnston et al. 1992; Kaspi et al. 1994). With around 50 HMXBs discovered in the LMC, we chose to target some of these sources in view of finding unexpected pulsed radio emission (Antoniou & Zezas 2016; Maitra et al. 2019; Haberl et al. 2022).

---

[3] http://simbad.u-strasbg.fr/simbad/

[4] https://github.com/telegraphic/pygdsm accessed on 2023 October 3

3.3 Globular clusters

GCs exhibit a significantly larger pulsar population per unit of stellar mass than the Milky Way disc, estimated to be approximately one hundred times greater and predominantly comprised of MSPs (Clark 1975; Katz 1975; Abbate 2021). This arises due to the conducive conditions of high-stellar densities in GCs, where there is a higher probability for isolated NSs forming binaries and being recycled to MSPs than elsewhere in the Milky Way. With over 150 identified Milky Way GCs, over 300 pulsars have been discovered within 44 of these clusters through various surveys[5] (e.g. Ransom et al. 2005; Pan et al. 2021), with a significant proportion discovered by MeerKAT (e.g. Ridolfi et al. 2021, 2022; Abbate et al. 2022; Chen et al. 2023). Notably, the LMC is home to more than a dozen GCs having ages surpassing 11 Gyr (Piatti, Alfaro & Cantat-Gaudin 2019), increasing the likelihood of hosting recycled pulsars. Therefore, we targeted some LMC GCs to enhance our chances of discovering binary systems, including MSP binaries.

3.4 Pulsar wind nebulae

PWNe are created through the interaction between outflowing winds emitted by a pulsar and the surrounding interstellar material and they can reside within SNRs. The presence of a pulsar within a SNR can be inferred by observing the interactions of its pulsar wind with the surrounding environment (e.g. Scargle 1969; Gaensler et al. 2002; Bietenholz et al. 2004). Two LMC pulsars are located within PWNe, namely PSRs J0540−6919 (Manchester et al. 1993b; Gotthelf & Wang 2000), and J0537−6910 (Wang et al. 2001). Additionally, there are three PWNe in the LMC without associated pulsars. These are situated in SNRs LHG 1 (Gaensler et al. 2003), DEM N206 (Williams et al. 2005), and L241 (Bamba et al. 2006). We aim to observe these PWNe to detect potential associated pulsars over the course of our survey of the LMC.

4 OBSERVATIONS

4.1 Set-up

We used the relative positions and the size of the MeerKAT primary beam, the incoherent beam (hereafter IB) which is about 1.1 deg in diameter at the half-power beam width (HPBW) at the *L*-band centre frequency (Asad et al. 2021), to group the selected sources together. The pointing centres were fine-tuned to encompass the maximum number of candidate sources within the IB (as described in Section 3). Thereafter, we used the MOSAIC software (Chen et al. 2021) to simulate coherent beam (hereafter, CB) maps, consisting of up to 768 beams (see later in this section), for our planned observations, and tiled the sources depending on their apparent sizes in the sky. The central region of the IB, where the sensitivity is highest, was tiled with the remaining CBs that were not targeting any specific source. Typically, to be more sensitive to pulsars, we used a 70 per cent overlap between neighbouring beams for SNRs and 50 per cent for remaining sources. An overlap value of 50 per cent implies that the neighbouring beams intersect at the point where their sensitivity is reduced to half of their maximum. Table 2 shows the LMC sources observed in the first four pointings of the survey. We also targeted known radio pulsars that fall within the four pointings, namely PSRs J0519−6932, J0535−6935,

---

[5]https://www3.mpifr-bonn.mpg.de/staff/pfreire/GCpsr.html accessed on 2024 July 11

Table 2. List of sources targeted in the four pointings, excluding known radio pulsars.

Object	Type	Pointing
N 120A	SNR	
LHG 27	SNR	
N 132D	SNR	
OGLE-CL LMC 318	GC	Pointing 1
XMMU J052016.0−692505	HMXB	
LXP8.04	HMXB	
HP 791	SNR	
MCSNR J0508−6830	SNR	
N 103B	SNR	
MCSNR J0507−6847	SNR	Pointing 2
RX J050736−6847.8	HMXB	
LXP169	HMXB	
SN 1987A	SNR	
Honeycomb	SNR	
MCSNR J0536−6913	SNR	
30 Dor B	SNR	Pointing 3
N 158A	SNR	
MCSNR J0538−6921	Candidate SNR	
PSR J0537−6910	PSR	
N 112	SNR	
LHG 26	SNR	
HP 700	SNR	Pointing 4
BRHT 33b	GC	
RXJ0516.0−6916	HMXB	

J0537−69, and J0540−6919. The detections of these pulsars give us an indication of the performance of the survey pipeline, as well as information about radio frequency interference (RFI) present during the observations. Fig. 1 shows the beam tilings for the four observed pointings.

The TRAPUM backend was used to record, store, and analyse the data taken for each observation. It comprises two user-supplied equipment (USE) backends provided by the Max-Planck-Institut-für-Radioastronomie (MPIfR) and the Max-Planck-Gesellschaft, namely the Filterbanking Beamformer User Supplied Equipment (FBFUSE; Barr 2018) and the Accelerated Pulsar Search User Supplied Equipment (APSUSE; see Padmanabh et al. 2023, and references therein). FBFUSE is an advanced beamformer that can produce digitally steerable CBs in real-time, and it is set up to record data in multiples of 4 antennas at a time to be efficient. The data are captured in a filterbank format by APSUSE, a high-end computing cluster that shares its storage with FBFUSE, where they are stored. Each USE has nodes that are capable of both GPU-based and CPU-based processing. We used the core of MeerKAT, comprising 44 antennas clustered over a 1 km radius, as it provides a favourable trade-off between sensitivity and beam coverage (Chen et al. 2021). Depending on availability, either 40 or 44 antennas were used for our observations. The observations were carried out using the *L*-band receiver, with frequencies 856–1712 MHz, a bandwidth of 856 MHz, and a central frequency of 1284 MHz. The four pointings were observed on 2022 September 08 (pointings 1 and 2) and on 2023 January 20 (pointings 3 and 4). The data were recorded with 2048 frequency channels and a sampling time of 153 µs, enabling FBFUSE to form up to 768 'tied-array' CBs. A summary of the observation parameters is given in Table 3.
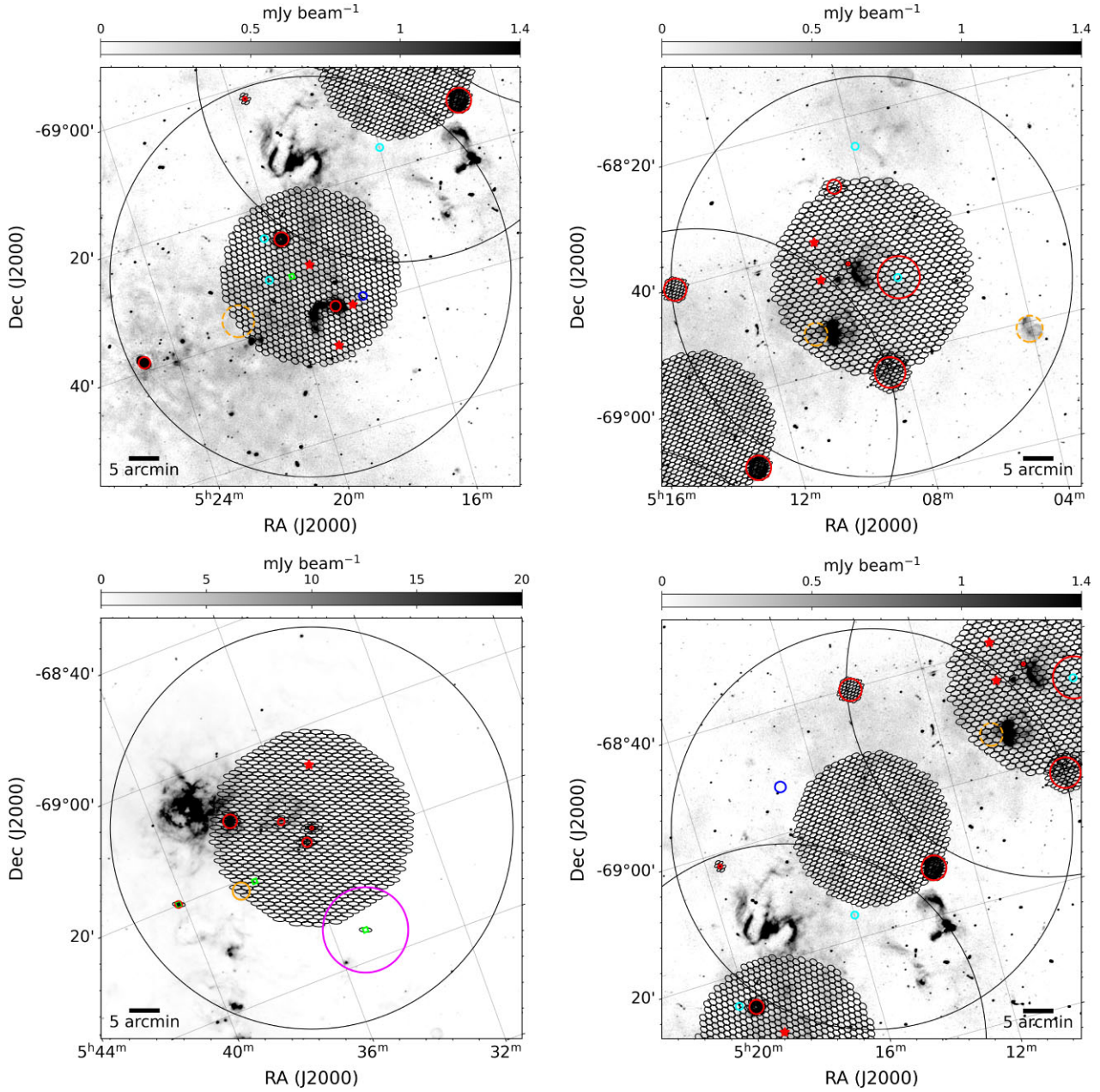
Figure 1. Beam maps, made with the PYTHON package APLPY (Robitaille & Bressert 2012), for Pointing 1 (upper left), Pointing 2 (upper right), Pointing 3 (lower left), and Pointing 4 (lower right), are shown overlaid onto an ASKAP 888 MHz radio continuum survey image from Pennock et al. (2021). The outermost black circle is the size of the IB of MeerKAT at the HPBW at 1284 MHz. The central tilings of CBs in black have a 50 per cent overlap, while the remaining tilings, depending on the source of interest, may have either a 50 or 70 per cent overlap (see Section 4.1). The red circles are SNRs, the green squares represent known pulsars, the blue circles are GCs, the cyan circles indicate HMXBs, and the orange circles are candidate SNRs (see Section 3 and Table 2). The dashed orange circles in Pointings 1 and 2 show candidate SNRs J0504−6901, J0510−6853, and J0521−6936 from Bozzetto et al. (2023) and Zangrandi et al. (2024), which had not yet been discovered at the time of observation. In Pointing 1, the SNR N 132D, found at its bottom left, was not tiled due to its proximity to the HPBW of the IB. The pink circle in Pointing 3 represents the error on the position of the known pulsar PSR J0535−6935 (Crawford et al. 2001). We did not detect this pulsar, possibly because it could be located outside of the CB tilings. The IB of Pointing 3 was centred on the SN 1987A remnant. The red star markers represent the new pulsar discoveries excluding the incoherent beam pulsar.

4.2 Survey sensitivity

Compared to Murriyang, MeerKAT has approximately four times the antenna gain at ∼2.8 K Jy^{-1} (Bailes et al. 2020) for the full array. To assess the differences in sensitivity among various LMC surveys, we employ the modified radiometer equation (1). This delineates a telescope's sensitivity in detecting radio signals, providing the

minimum detectable flux density, S_{min}, for a pulsar with a spin period, P, and effective pulse width, W. It is formulated as (Dewey et al. 1985; Lorimer & Kramer 2005):

$$S_{\mathrm{min}} = \frac{\beta \, \mathrm{S/N} \, (T_{\mathrm{sys}} + T_{\mathrm{sky}})}{G \sqrt{n_{\mathrm{pol}} \, t_{\mathrm{obs}} \, \Delta \nu}} \sqrt{\frac{W}{P - W}}. \tag{1}$$

Table 3. List of parameters for the four MeerKAT pointings. The coherent beams' major and minor axes are given in arcseconds, along with the position angles, which are measured from East to North on the sky (Chen et al. 2021; Bezuidenhout et al. 2023).

Observation Date	Pointing centre	CB dishes (number of CBs)	IB dishes	CB size	Observation duration
Pointing 1 2022 Sept 08	$05^h19^m13^s00$ $-69°33'20''00$	40 (759)	59	$39.66''$, $29.20''$, $-50.37°$	7172.50 s
Pointing 2 2022 Sept 08	$05^h08^m23^s40$ $-68°46'35''00$	40 (762)	59	$50.33''$, $30.40''$, $-4.40°$	7176.89 s
Pointing 3 2023 Jan 20	$05^h35^m28^s02$ $-69°16'11''10$	44 (764)	62	$61.70''$, $22.99''$, $-24.09°$	7160.58 s
Pointing 4 2023 Jan 20	$05^h14^m46^s19$ $-69°03'19''20$	44 (766)	62	$41.27''$, $23.16''$, $7.82°$	7178.77 s

For our survey, the S/N of the detected pulse is taken to be 9.5, which is our minimum spectral S/N cut (see Section 4.3), the system temperature contribution, T_{sys}, is 18 K (Bailes et al. 2020), the sky temperature contribution, T_{sky}, is 4.6 K (Price 2016; Zheng et al. 2017), the sensitivity degradation factor due to the signal digitization, β, is 1.0 for 8-bit digitization (Kouwenhoven & Voûte 2001), G is the antenna gain taken to be 1.84 K Jy^{-1} for MeerKAT's core, $n_{pol} = 2$ is the number of orthogonal polarizations to be summed, t_{obs} is the observing time, and $\Delta\nu$ is the total bandwidth.

Fig. 2 shows a comparison between the sensitivity curves of previous LMC pulsar surveys and this survey overlaid with the discovery flux densities of known LMC radio pulsars at 1400 MHz ($S_{1400\ MHz}$). The S/N thresholds were found from their respective papers, or assumed using our best knowledge of the surveys. We used a folded S/N threshold of 10 for McConnell et al. (1991), a spectral S/N threshold of 7 for both Crawford et al. (2001) and Manchester et al. (2006), and a folded S/N threshold of 8 for Ridley et al. (2013) and Hisano et al. (2022). Therefore, the sensitivity of each survey does not scale directly with the telescope parameters. We made use of a Fast Fourier Transform (FFT) efficiency factor of 0.7 to convert between spectral S/N and folded S/N (Morello et al. 2020). We used a sensitivity degradation factor due to digitization of 1.06 for the High Resolution LMC Survey (Ridley et al. 2013 and Hisano et al. 2022), which makes use of BPSR's 2-bit digitization, and 1.25 for surveys using 1-bit digitization (McConnell et al. 1991, Crawford et al. 2001, and Manchester et al. 2006). All of the Murriyang surveys had a gain assumed to be 0.735 K Jy^{-1} (Manchester et al. 2001), and a sky temperature of 4.1 K, except for McConnell et al. (1991), which had a sky temperature of 17.8 K due to a different centre frequency of 610 MHz, compared to 1374 MHz for the others (Price 2016; Zheng et al. 2017). We assumed a radio power-law spectral index of -1.6 ± 0.54 (Jankowski et al. 2018) for converting the minimum flux densities of the surveys to $S_{1400\ MHz}$. The shaded regions in Fig. 2 capture the uncertainty range corresponding to the radio power-law spectral index. The system temperature was assumed to be 44 K based on McCulloch et al. (1983) for McConnell et al. (1991), and 21 K according to Manchester et al. (2001) for both Crawford et al. (2001) and Manchester et al. (2006). For the High Resolution LMC Survey, the system temperature was taken to be 23 K (Keith et al. 2010). Where the effective pulse widths and pulsar flux densities for the different surveys were not available in the literature, we assumed an intrinsic pulse width of 2.5 per cent of the pulsar period and considered additional contributions to the observed pulse width to obtain the flux densities. These included the DM smearing, τ_{DM}, the survey sampling time, τ_{samp}, and the scattering time-scale, τ_{scatt}. The
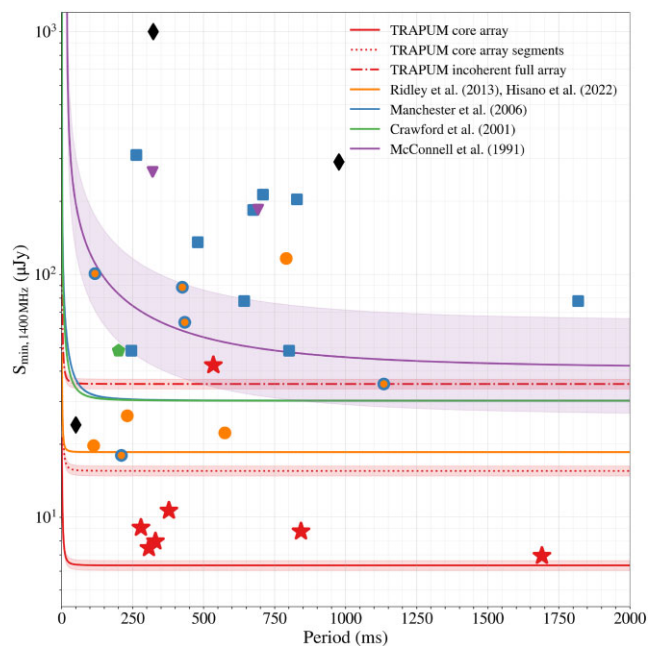

Figure 2. The minimum flux densities at 1400 MHz of the PMPS, the High Resolution LMC Survey, and this work are plotted against pulse period. The shaded regions around the sensitivity curves indicate the ranges of minimum flux density fluctuations, reflecting the pulsar power-law spectral index uncertainty as per Jankowski et al. (2018), which is -1.6 ± 0.54. The minimum flux densities using Murriyang are slightly better than the literature, but this is based on our best knowledge of the surveys (see Section 4.2). We note that the horizontal section of each of the minimum density curves excludes the red noise contribution, which is known to impact slow pulsars at longer integrations (e.g. Lazarus et al. 2015; van Heerden, Karastergiou & Roberts 2017). Each of the markers, denoting the 24 radio pulsars discovered in the LMC, has a colour corresponding to the publication where the discovery was documented. The black diamond markers represent the flux densities for PSRs J0523−7125 (Wang et al. 2022), J0529−6652 (Crawford et al. 2001), and J0540−6919 (Johnston et al. 2004). Notably, these pulsars have not been discovered in the main LMC pulsar surveys outlined in this paper. There are five orange circle markers with a blue outline representing pulsars which were reported in Ridley et al. (2013) but discovered in the reprocessed archival PMPS data. One of these 5 blue-outlined orange circles, PSR J0535−66, has a 1400 MHz flux density below the minimum flux densities of the Murriyang surveys, which is due to it being discovered using an integration time of 14400 s (Ridley et al. 2013). The newly discovered pulsars are represented by the red star markers, with the incoherent beam pulsar having the highest flux density (see Section 6).

latter was based on the model by Bhat et al. (2004). We used the median DM of the known LMC pulsars of 98.7 pc cm^{-3} for these calculations and a radio power-law spectral index of -1.6 to convert the flux densities of the known pulsars to $S_{1400 \text{ MHz}}$. A 2-h observation with the MeerKAT core achieves a deeper flux sensitivity limit than the PMPS and the High Resolution LMC Survey. For periods greater than 50 ms, our survey achieves $\sim$3 times the sensitivity of the High Resolution LMC Survey, reaching down to a limiting flux density, i.e. the faintest signal that can be detected from a radio pulsar located at the centre of both the IB and a CB, of 6.3 μJy at 1400 MHz.

4.3 Search

The TRAPUM pulsar search pipeline consisted of three processes: searching, filtering, and folding. The search process involved the removal of RFI using `filtool` from the PULSARX[6] suite (Men et al. 2023). A de-dispersion plan was created using `DDplan.py` from the PRESTO package (Ransom 2011). We chose a DM range of 35–500 pc cm^{-3}, given that for the known pulsars in the LMC, the lowest DM is 45 pc cm^{-3} and the highest is 273 pc cm^{-3} (see Table 1). This de-dispersion plan, with step sizes of 0.1 up to a DM of 334 pc cm^{-3}, and 0.2 at higher DM values, was fed into the search pipeline where PEASOUP[7] (Barr 2020), a GPU-based acceleration search software suite, performed the de-dispersion and the periodicity search (Morello et al. 2019). We configured PEASOUP to search for candidates with periods up to a maximum of 10 s. To increase our sensitivity to pulsars located in binaries with shorter orbital periods where the latter can induce Doppler shifts on the signals causing pulse smearing, the 2-h observation for each pointing was divided into six segments of 20-min each and a linear acceleration search was performed on each segment. For pointings 1 and 2, the acceleration search range was chosen to be -50 to 50 ms^{-2}, with an acceleration tolerance of 10 per cent for the segment searches, while for pointings 3 and 4, to cut down on processing time, we did not perform any acceleration search. The acceleration tolerance parameters ensure the pulse smearing due to acceleration step size stays within ten per cent of total smearing effects (Levin 2012). The spectral S/N threshold of the FFT was set to be 8 with a maximum of 8 harmonics summed.

After completing the search, we subjected the candidates to a filtering process using CANDIDATE_FILTER[8] This filter sifted known RFI signals and then clustered candidates considering spin periods, DMs, beam location, and acceleration values. Through this method, we effectively separated RFI signals, which tend to manifest across the entire field of view, from possible pulsar signals.

Following the filtering, the candidates were folded by making use of `psrfold_fil`, a component of the PULSARX package. It used the DMs, spin periods, and acceleration values of the candidates derived from the search. Candidates with a spectral S/N above 9 were folded for pointings 1 and 2, while for pointings 3 and 4, a higher S/N threshold of 9.5 was used. This modification was made to optimize pipeline processing speed, reducing the number of candidates to fold, while maintaining our pulsar detection capabilities. We plan to keep the spectral S/N threshold as 9.5 for future pointings. Similarly, due to the high number of candidates,
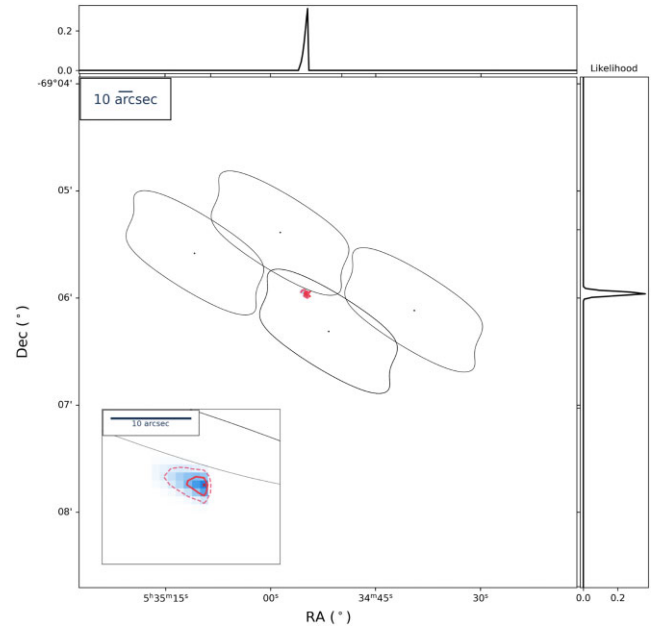

Figure 3. The localization of PSR J0534$-$6905 using SEEKAT, where the pulsar was detected in four beams, shown by the black outlines. The inset plot on the bottom left provides a zoomed-in view of the maximum-likelihood position, which is indicated by a red cross. The 1σ and 2σ errors on the position (see Table 4) are demarcated by the red continuous line and the red dashed line, respectively.

we applied a lowest period cut-off of 8 times the sampling time, i.e. 1.216 ms.

The output files containing pulsar candidates generated by the folding process were archive files that are compatible with the PSRCHIVE package (Hotan, van Straten & Manchester 2004; van Straten, Demorest & Oslowski 2012). These files were then classified using the Pulsar Image-based Classification System (PICS; Zhu et al. 2014), which employs deep neural networks for image pattern recognition in pulsar detection. PICS was trained using the Pulsar Arecibo L-band Feed Array (PALFA) survey data (Cordes et al. 2006), along with data from TRAPUM pulsar surveys (Padmanabh et al. 2023). PICS assigned a number ranging from 0 to 1 to the candidates, a proxy for probability, with a higher score implying that the candidate showed characteristics more akin to those of a pulsar.

The resulting candidates having altogether a folded S/N above 7, a DM greater than 3, and a PICS score above 0.1 were then viewed using CANDYJAR[9], enabling quick sorting and manual classification. Once we identified a candidate as an actual pulsar, we refolded the surrounding beams with the candidate parameters to verify additional detections for confirmation. The SEEKATPYTHON package[10] (hereafter SEEKAT; Bezuidenhout et al. 2023) improved localization using these detections (see Fig. 3), requiring a minimum of three detections to do so. It makes use of the S/N, the point spread function (PSF), and the location of the beams with detections to triangulate a position for a pulsar on the sky. We also refolded the detection beam of a pulsar using integer multiples of the pulsar period to potentially improve the discovery S/N ratio and accommodate for harmonics. A

---

[6]https://github.com/ypmen/PulsarX accessed on 2022 September 12

[7]https://github.com/ewanbarr/peasoup accessed on 2022 September 12

[8]https://github.com/prajwalvp/candidate_filter accessed on 2022 September 20

[9]https://github.com/vivekvenkris/CandyJar accessed on 2022 October 4

[10]https://github.com/BezuidenhoutMC/SeeKAT accessed on 2022 November 6

full description of the search pipeline can be found in Padmanabh et al. (2023) and Carli et al. (2024).

5 RESULTS

The first four pointings of the TRAPUM LMC Survey have yielded seven new pulsars, with four in Pointing 1, two in Pointing 2, and one in Pointing 3. In Pointing 1, one of the pulsars was only detected in the IB and therefore has poor localization. We call this pulsar the incoherent beam pulsar, or IB pulsar for short, for the remainder of this work.

The periods of the pulsars range from 278 to 1690 ms, categorizing them as 'slow' pulsars, or normal pulsars. They have DMs ranging from 79 to 254.2 pc cm^{-3}, and if we consider the DM contribution from the Milky Way in the direction of the LMC, which is about 53 pc cm^{-3} using the NE2001 electron density model (Cordes 2004), and about 58 pc cm^{-3} using the YMW16 electron density model (Yao, Manchester & Wang 2017), we can conclude that these pulsars are extragalactic and belong to the LMC. The DM range of the new pulsars is also consistent with the previously discovered LMC pulsars, which have DMs between 45 pc cm^{-3}, which notably contradicts the estimations of the electron density models, and 273 pc cm^{-3} (see Table 1). We performed follow-up observations of the new pulsars discovered in pointings 1 and 2, and all of the pulsars were detected again except for the incoherent beam pulsar. The IBs of the follow-up observations were unfortunately not analysed to enable the confirmation of the incoherent beam pulsar, due to the requirement to rapidly delete data. It was also not detected in the IB of Pointing 4, despite the latter overlapping with that of Pointing 1 (see Fig. 1) when processed using the search pipeline. All of the already known pulsars that were located within our pointings (see Section 4.1) were successfully detected, with the exception of PSR J0535−6935 (see Fig. 1). We did not detect any pulsed radio emission from the observation of the SN 1987A remnant and the X-ray pulsar PSR J0537−6910 in Pointing 3 (see discussion in Section 6).

The integrated pulse profiles for the seven pulsars are shown in Fig. 4, and they all have a single pulse profile. To determine the pulse width of each new discovery, we made a noise-less pulse template for each pulsar using the PAAS tool from PSRCHIVE, and we simulated 1000 noise profiles using the off-pulse noise statistics derived from their respective average pulse profiles. We fitted von Mises functions to each pulse profile for every simulated noise profile using the `fitvonMises` routine from PSRSALSA[11] (Weltevrede 2016), which allowed us to measure the pulse widths at 50 per cent of the peak intensity, W_{50}, without being significantly influenced by noise. The W_{50} for each pulsar was obtained by taking the average of the 1000 resultant pulse width measurements. Table 4 provides a summary of the properties of the new pulsars and their derived parameters.

5.1 Discoveries

5.1.1 PSR J0509−6838

PSR J0509−6838 was discovered with a folded S/N of 10.3, obtained from PulsarX (see Section 4.3), in the complete 2-h observation data of Pointing 2, making it the weakest detection out of the seven new discoveries. It was found within a beam of the central tiling of Pointing 2 (see Fig. 1), and further detected in the complete 2-h data

[11] https://github.com/weltevrede/psrsalsa accessed on 2023 October 25

of two surrounding beams, enabling its localization using SEEKAT. With a period of 278.75 ms, it is the fastest rotating pulsar amongst the seven new discoveries. The W_{50} is (19.4 ± 2.7) ms, corresponding to a duty cycle of 7 per cent.

5.1.2 PSR J0509−6845

PSR J0509−6845 was discovered with a folded S/N of 13.9 in the complete 2-h observation data of Pointing 2. It was detected within a beam of the central tiling of Pointing 2, with only one additional detection found in the 2-h data of the surrounding beams. Consequently, we were unable to achieve a localization more precise than the size of the coherent beam in which it was detected. The W_{50} is (8.4 ± 0.8) ms, resulting in a duty cycle of 2.7 per cent.

5.1.3 PSR J0518−6939

PSR J0518−6939 was discovered with a folded S/N of 16.6 in the complete 2-h observation data of Pointing 1. It was found within a beam of the central tiling of Pointing 1 (see Fig. 1), and further detected in the complete 2-h data of two surrounding beams, enabling its localization using SEEKAT. PSR J0518−6939 has a DM of 254.20 pc cm^{-3}, which is the second-highest DM in the LMC, after PSR J0537−69 with a DM of 273 pc cm^{-3} (see Table 1). The W_{50} is (7.3 ± 0.7) ms, corresponding to a duty cycle of 2.2 per cent.

5.1.4 PSR J0518−6946

PSR J0518−6946 was discovered with a folded S/N of 13.9 in the complete 2-h observation data of Pointing 1. It was located within a beam of the central tiling. The pulsar was further detected in the complete 2-h data of two surrounding beams, enabling its localization using SEEKAT. PSR J0518−6946 has a period of 1.69 s, making it the second-longest period radio pulsar in the Magellanic Clouds, following PSR J0534−6845 with a period of 1.82 s (see Table 1). The W_{50} is (40 ± 3) ms, resulting in a duty cycle of 2.4 per cent.

5.1.5 PSR J0519−6931

PSR J0519−6931 was discovered with a folded S/N of 23.4 in the complete 2-h observation data of Pointing 1, making it the strongest detection amongst the seven new discoveries. It was found within a beam of the central tiling, with only one additional detection found in the 2-h data of the surrounding beams. With a total of two detections, we were unable to obtain a better localization than the size of the coherent beam in which it was detected. The W_{50} is (7.5 ± 0.4) ms, corresponding to a duty cycle of 2 per cent.

5.1.6 Incoherent beam pulsar

The incoherent beam pulsar was discovered with a folded S/N of 11.0 in the complete 2-h observation data of Pointing 1. It was located outside of the beam tilings of Pointing 1, with a period of 533.97 ms and a DM of 79 pc cm^{-3}. The W_{50} is (24 ± 3) ms, resulting in a duty cycle of 4.5 per cent.

5.1.7 PSR J0534−6905

PSR J0534−6905 was discovered with a folded S/N of 17.4 in the complete 2-h observation data of Pointing 3. It was found within a beam of the central tiling (see Fig. 1), and further detected in
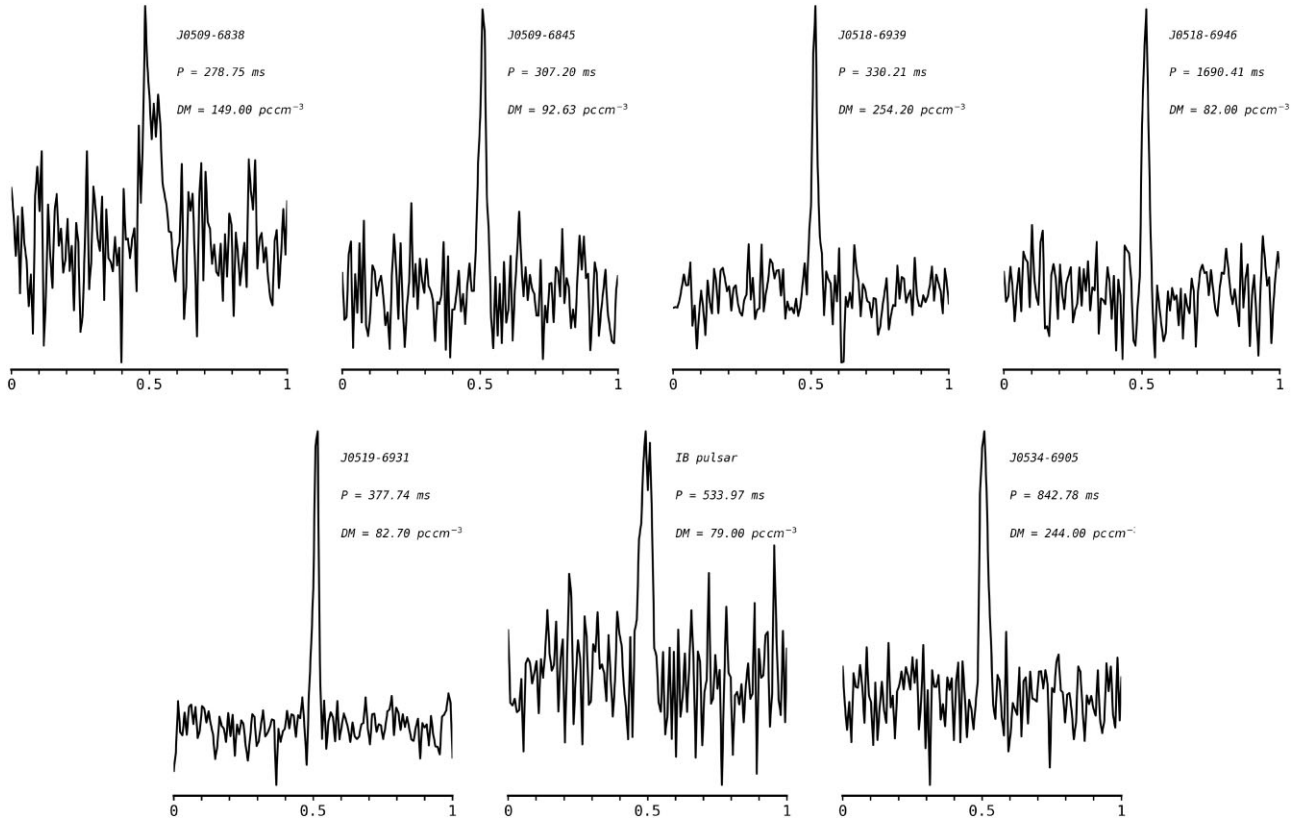
Figure 4. The integrated pulse profiles, along with the periods and DMs, of the newly discovered pulsars within MeerKAT's *L*-band, with each plot representing one full rotation of the pulsar with 128 phase bins. The effective time resolution for each pulsar was less than its pulse width.

Table 4. Properties of the seven new pulsars, including the discovery flux density values (see Section 4.2) and the pulse widths at 50% of the peak intensity. The quoted uncertainties in parentheses are on the last digit. The error in each position is the 2σ output by SEEKAT (see Fig. 3). For the pulsars denoted by a ∗, the error in their positions are the sizes of the CBs in which they were found (see Table 3). The RA and Dec. of the incoherent beam pulsar are the same as the centre of Pointing 1.

Pulsar (J2000)	RA	Dec.	DM (pc cm^{-3})	Period (ms)	Epoch (MJD)	S/N	W_{50} (ms)	$S_{1400\,\mathrm{MHz}}$ (μJy)
J0509−6838	$05^{\mathrm{h}}09^{\mathrm{m}}58\overset{\mathrm{s}}{.}17\,^{+3.0}_{-1.8}$	$-68°38'46''00\,^{+8.6}_{-16.0}$	149(2)	278.75363(26)	59830.4	10.3	19.4(27)	9.1
J0509−6845∗	$05^{\mathrm{h}}09^{\mathrm{m}}55\overset{\mathrm{s}}{.}26$	$-68°45'09''50$	92.63(47)	307.197131(77)	59830.4	13.9	8.4(8)	7.5
J0518−6939	$05^{\mathrm{h}}18^{\mathrm{m}}15\overset{\mathrm{s}}{.}50\,^{+1.0}_{-0.7}$	$-69°39'45''20\,^{+4.5}_{-6.3}$	254.20(32)	330.209968(56)	59830.3	16.6	7.3(7)	8.0
J0518−6946	$05^{\mathrm{h}}18^{\mathrm{m}}58\overset{\mathrm{s}}{.}39\,^{+1.1}_{-1.6}$	$-69°46'16''75\,^{+5.3}_{-5.5}$	82(3)	1690.4142(25)	59830.3	13.9	40(3)	6.9
J0519−6931∗	$05^{\mathrm{h}}19^{\mathrm{m}}08\overset{\mathrm{s}}{.}39$	$-69°31'25''60$	82.70(26)	377.735862(52)	59830.3	23.4	7.5(4)	10.6
Incoherent beam	$05^{\mathrm{h}}19^{\mathrm{m}}13\overset{\mathrm{s}}{.}00$	$-69°33'20''00$	79(2)	533.96689(51)	59830.3	11.0	24(3)	42.3
J0534−6905	$05^{\mathrm{h}}34^{\mathrm{m}}54\overset{\mathrm{s}}{.}69\,^{+0.0}_{-0.9}$	$-69°05'57''90\,^{+2.0}_{-2.0}$	244(1)	842.78252(58)	59964.6	17.4	25(2)	8.8

the complete 2-h data of three surrounding beams, enabling its localization using SEEKAT (see Fig. 3). The W_{50} is (25 ± 2) ms, corresponding to a duty cycle of 3 per cent.

6 DISCUSSION AND CONCLUSIONS

The seven radio pulsars discovered increase the known LMC pulsar population to 32, an increase of ∼30 per cent. They do not seem to be associated with any of the sources listed in Table 2. We cross-checked the positions with the ASKAP 888 MHz radio continuum survey image of the LMC (Pennock et al. 2021), and we found that PSR J0518−6946 seems to be located within a faint shell of radio

emission, possibly linked to the nearby SNR N 120A, although this is not conclusive, with an on-sky angular separation of ∼432 arcsec from the centre of the latter. Similarly, PSR J0518−6939 is also located in a region of radio emission, closer to SNR N 120A. The on-sky angular separation in this case is ∼150 arcsec. If PSR J0518−6939 is associated with SNR N 120A, which has an estimated age of 7300–8000 yr (Rosado et al. 1993; Reyes-Iturbide, Rosado & Velázquez 2008), it would have a maximum average transverse velocity of over 4000 km s^{-1}, one order of magnitude higher than the mean velocity of young pulsars, which we take to be ∼400 km s^{-1} (Lyne & Lorimer 1994; Hobbs et al. 2005; Verbunt, Igoshev & Cator 2017), and several times higher than the fastest

moving pulsars, around $1000 \, \text{km s}^{-1}$ (Chatterjee et al. 2005; Deller et al. 2019), making the association unlikely. PSR J0534$-$6905 has a high DM of $244 \, \text{pc cm}^{-3}$, which can be explained by its location on the outskirts of the star-forming region, 30 Doradus, where there is abundant gas and dust. Future LMC imaging surveys may reveal more about these pulsars and their associations.

The incoherent beam pulsar was detected with a $S_{1400 \, \text{MHz}}$ of $42.3 \, \mu\text{Jy}$ (see Table 4), which implies it is bright enough to have been detectable in the High Resolution LMC Survey and the PMPS, as seen in Fig. 2. A detection within the previous surveys' data would help in framing the localization and for this reason, we downloaded the Murriyang archival data available from the CSIRO Data Access Portal[12] centred on the coordinates of the IB of Pointing 1, and within a radius of 30 arcmin. We undertook a search using pdmp from PSRCHIVE around the discovery DM, with a range of $\pm 10 \, \text{pc cm}^{-3}$, and discovery period, with a range of ± 10 per cent. Unfortunately, the searches did not yield any detection of the incoherent beam pulsar within the Murriyang archival data. This could be due to many factors, such as the distribution of the beams of the Murriyang surveys, and variations in the pulsar flux density.

The observation of the SN 1987A remnant with MeerKAT was on day 13 115 after the explosion. The non-detection of radio pulsations from the SN 1987A remnant could mean that the putative NS is still shrouded in substantial clouds of matter. The impact of the surrounding nebula varies significantly with observing frequency, the structure of surrounding dust and gas, and the viewing angle. With time, the ejected material is expected to clear out and could possibly give a better line of sight view of the suspected NS. The ejecta dust from the supernova has not gone through any reverse shock-related changes and it is expected that this could cause some dissipation when it does happen (Jones et al. 2023). We determine the upper limit for the detection of pulsed radio emission in the SN 1987A remnant as $6.3 \, \mu\text{Jy}$ at 1400 MHz, since Pointing 3 was centred on the SN 1987A remnant (see Fig. 1). We plan to re-observe the SN 1987A remnant using the S-band receivers of MeerKAT, with frequencies 1.7–3.5 GHz (Barr 2018), to attempt to mitigate dispersion and scattering effects owing to the dust and gas clouds.

Crawford (2024) detected three repeated signals from PSR J0537$-$6910 at a DM of $103.4 \, \text{pc cm}^{-3}$. We used pdmp to search the CB data from Pointing 3 corresponding to the location of the X-ray pulsar around this DM value, with a range of $\pm 10 \, \text{pc cm}^{-3}$, and the pulsar period with a range of ± 10 per cent. We unfortunately did not detect any pulsed radio emission from PSR J0537$-$6910, allowing us to derive the upper limit as $7.7 \, \mu\text{Jy}$ at 1400 MHz, after correcting for the sensitivity loss due to the offset between the location of the pulsar and the centre of Pointing 3.

The seven new pulsars represent discoveries from the initial four pointings of the 28 currently planned for the TRAPUM LMC Survey conducted using MeerKAT. We save the low-resolution version of the data from all observed pointings for future Fast-Folding Algorithm searches. Follow-up timing observations are underway, and a detailed analysis will be presented in a future paper.

ACKNOWLEDGEMENTS

DATA AVAILABILITY

The discovery PSRCHIVE archive files of the new pulsars can be found on ZENODO at DOI 10.5281/zenodo.12723576. The TRAPUM collaboration will share the candidates list upon appropriate request.

REFERENCES

Abbate F., 2021, Searching for pulsars in globular clusters with the MeerKAT Radio Telescope. preprint (arXiv:2112.06528)
Abbate F. et al., 2022, MNRAS, 513, 2292
Agazie G. et al., 2023, ApJ, 956, L3
Alp D. et al., 2018, ApJ, 864, 174
Alpar M. A., Cheng A. F., Ruderman M. A., Shaham J., 1982, Nature, 300, 728
Antoniou V., Zezas A., 2016, MNRAS, 459, 528
Asad K. M. B. et al., 2021, MNRAS, 502, 2970
Baade W., Zwicky F., 1934, Proc. Natl. Acad. Sci., 20, 254
Badenes C., Maoz D., Draine B. T., 2010, MNRAS, 407, 1301
Bailes M. et al., 2020, Publ. Astron. Soc. Aust., 37, e028
Bamba A., Ueno M., Nakajima H., Mori K., Koyama K., 2006, A&A, 450, 585
Barr E. D., 2018, in Weltevrede P., Perera B. B. P., Preston L. L., Sanidas S., eds, Vol. 13, Proceedings of the International Astronomical Union 337, Pulsar Astrophysics the Next Fifty Years. p. f1
Barr E., 2020, Peasoup: C++/CUDA GPU pulsar searching library. Astrophysics Source Code Library, record ascl:2001.014, preprint(ascl:2001.014)
Basu A. et al., 2022, MNRAS, 510, 4049
Bezuidenhout M. C. et al., 2023, RAS Tech. Instrum., 2, 114
Bhat N. D. R., Cordes J. M., Camilo F., Nice D. J., Lorimer D. R., 2004, ApJ, 605, 759
Bietenholz M. F., Hester J. J., Frail D. A., Bartel N., 2004, ApJ, 615, 794
Bionta R. M. et al., 1987, Phys. Rev. Lett., 58, 1494
Bozzetto L. M. et al., 2017, ApJS, 230, 2
Bozzetto L. M. et al., 2023, MNRAS, 518, 2574
Burrows A., Lattimer J. M., 1987, ApJ, 318, L63
Camilo F. et al., 2018, ApJ, 856, 180
Carli E. et al., 2024, MNRAS, 531, 2835
Chatterjee S. et al., 2005, ApJ, 630, L61

[12] https://data.csiro.au/

Chen W., Barr E., Karuppusamy R., Kramer M., Stappers B., 2021, J. Astron. Instrum., 10, 2150013

Chen W. et al., 2023, MNRAS, 520, 3847

Choudhury S. et al., 2020, MNRAS, 497, 3746

Choudhury S. et al., 2021, MNRAS, 507, 4752

Cigan P. et al., 2019, ApJ, 886, 51

Clark G. W., 1975, ApJ, 199, L143

Cordes J. M., 2004, in Clemens D., Shah R., Brainerd T., eds, ASP Conf. Ser. Vol. 317, Milky Way Surveys: The Structure and Evolution of our Galaxy. Astron. Soc. Pac., San Francisco, p. 211

Cordes J. M. et al., 2006, ApJ, 637, 446

Crawford F., 2024, ApJ, 968, 99

Crawford F., Kaspi V. M., Manchester R. N., Lyne A. G., Camilo F., D'Amico N., 2001, ApJ, 553, 367

De Marchi G. et al., 2011, ApJ, 739, 27

Deller A. T. et al., 2019, ApJ, 875, 100

Dewey R. J., Taylor J. H., Weisberg J. M., Stokes G. H., 1985, ApJ, 294, L25

EPTA Collaboration, 2023, A&A, 678, A50

Fahrion K., De Marchi G., 2024, A&A, 681, A20

Fornasini F., Antoniou V., Dubus G., 2023, in Bambi C., eds, Handbook of X-ray and Gamma-ray Astrophysics. Springer, Singapore, p. 143

Fransson C. et al., 2024, Science, 383, 898

Gaensler B. M., Arons J., Kaspi V. M., Pivovaroff M. J., Kawai N., Tamura K., 2002, apj, 569, 878

Gaensler B. M., Hendrick S. P., Reynolds S. P., Borkowski K. J., 2003, ApJ, 594, L111

Gardner J. P. et al., 2006, Space Sci. Rev., 123, 485

Geyer M. et al., 2021, MNRAS, 505, 4468

Gotthelf E. V., Wang Q. D., 2000, ApJ, 532, L117

Graczyk D. et al., 2020, apj, 904, 13

Greco E. et al., 2022, ApJ, 931, 132

Grimm H. J., Gilfanov M., Sunyaev R., 2003, MNRAS, 339, 793

Haberl F. et al., 2012, A&A, 543, A154

Haberl F., Maitra C., Vasilopoulos G., Maggi P., Udalski A., Monageng I. M., Buckley D. A. H., 2022, A&A, 662, A22

Haskell B., Melatos A., 2015, Int. J. Mod. Phys. D, 24, 1530008

Hirata K. et al., 1987, Phys. Rev. Lett., 58, 1490

Hisano S. et al., 2022, apj, 928, 161

Hobbs G., Lorimer D. R., Lyne A. G., Kramer M., 2005, MNRAS, 360, 974

Hotan A. W., van Straten W., Manchester R. N., 2004, PASA, 21, 302

Jankowski F., van Straten W., Keane E. F., Bailes M., Barr E. D., Johnston S., Kerr M., 2018, MNRAS, 473, 4436

Johnston S., Romani R. W., 2003, ApJ, 590, L95

Johnston S., Manchester R. N., Lyne A. G., Bailes M., Kaspi V. M., Qiao G., D'Amico N., 1992, ApJ, 387, L37

Johnston S., Romani R. W., Marshall F. E., Zhang W., 2004, MNRAS, 355, 31

Johnston S. et al., 2022, MNRAS, 509, 5209

Jonas J., MeerKAT Team, 2016, MeerKAT Science: On the Pathway to the SKA. p. 1

Jones O. C. et al., 2023, ApJ, 958, 95

Kaspi V. M., Johnston S., Bell J. F., Manchester R. N., Bailes M., Bessell M., Lyne A. G., D'Amico N., 1994, ApJ, 423, L43

Katz J. I., 1975, Nature, 253, 698

Kavanagh P. J., Sasaki M., Filipović M. D., Points S. D., Bozzetto L. M., Haberl F., Maggi P., Maitra C., 2022, MNRAS, 515, 4099

Keith M. J. et al., 2010, MNRAS, 409, 619

Kim V., Izmailova I., Aimuratov Y., 2023, ApJS, 268, 21

Kouwenhoven M. L. A., Voûte J. L. L., 2001, A&A, 378, 700

Lazarus P. et al., 2015, ApJ, 812, 81

Levin L., 2012, PhD thesis, Swinburne University of Technology, Australia

Liu Q. Z., van Paradijs J., van den Heuvel E. P. J., 2005, A&A, 442, 1135

Lorimer D. R., Kramer M., 2005, Handbook of Pulsar Astronomy. Cambridge Univ. Press, Cambridge, p. 265

Lyne A., 1999, in Arzoumanian Z., Van der Hooft F., van den Heuvel E. P. J., eds, Pulsar Timing, General Relativity and the Internal Structure of Neutron Stars. Koninklijke Nederlandse Akademie van Wetenschappen, p. 141

Lyne A. G., Lorimer D. R., 1994, Nature, 369, 127

Maitra C. et al., 2019, MNRAS, 490, 5494

Maitra C., Haberl F., Maggi P., Kavanagh P. J., Vasilopoulos G., Sasaki M., Filipović M. D., Udalski A., 2021, MNRAS, 504, 326

Manchester R. N., Peterson B. A., 1996, ApJ, 456, L107

Manchester R. N., Mar D. P., Lyne A. G., Kaspi V. M., Johnston S., 1993a, ApJ, 403, L29

Manchester R. N., Staveley-Smith L., Kesteven M. J., 1993b, ApJ, 411, 756

Manchester R. N. et al., 2001, MNRAS, 328, 17

Manchester R. N., Hobbs G. B., Teoh A., Hobbs M., 2005, AJ, 129, 1993

Manchester R. N., Fan G., Lyne A. G., Kaspi V. M., Crawford F., 2006, ApJ, 649, 235

Marshall F. E., Gotthelf E. V., Zhang W., Middleditch J., Wang Q. D., 1998, ApJ, 499, L179

Marshall F. E., Guillemot L., Kust Harding A., Martin P., Smith D. A., 2016, American Astronomical Society Meeting Abstracts #227. p. 423.04

Matteucci F., 2014, in Bland-Hawthorn J., Freeman K., Matteucci F., eds, Vol. 37, Saas-Fee Advanced Course The Origin of the Galaxy and Local Group. Springer-Verlag, Berlin Heidelberg, p. 145

McConnell D., McCulloch P. M., Hamilton P. A., Ables J. G., Hall P. J., Jacka C. E., Hunt A. J., 1991, MNRAS, 249, 654

McCulloch P. M., Hamilton P. A., Ables J. G., Hunt A. J., 1983, Nature, 303, 307

Men Y., Barr E., Clark C. J., Carli E., Desvignes G., 2023, A&A, 679, A20

Middleditch J., Pennypacker C., 1985, Nature, 313, 659

Morello V. et al., 2019, MNRAS, 483, 3673

Morello V., Barr E. D., Stappers B. W., Keane E. F., Lyne A. G., 2020, MNRAS, 497, 4654

Padmanabh P. V. et al., 2023, MNRAS, 524, 1291

Pakmor R. et al., 2022, MNRAS, 512, 3602

Pan Z. et al., 2021, ApJ, 915, L28

Papitto A. et al., 2013, Nature, 501, 517

Pennock C. M. et al., 2021, MNRAS, 506, 3540

Piatti A. E., Alfaro E. J., Cantat-Gaudin T., 2019, MNRAS, 484, L19

Price D. C., 2016, PyGSM: Python interface to the Global Sky Model. Astrophysics Source Code Library, record ascl:1603.013, preprint(ascl:1603.013)

Radhakrishnan V., Srinivasan G., 1982, Curr. Sci., 51, 1096

Ransom S., 2011, PRESTO: PulsaR Exploration and Search TOolkit, Astrophysics Source Code Library, record ascl:1107.017, preprint(ascl:1107.017)

Ransom S. M., Hessels J. W. T., Stairs I. H., Freire P. C. C., Camilo F., Kaspi V. M., Kaplan D. L., 2005, Science, 307, 892

Reardon D. J. et al., 2023, ApJ, 951, L6

Reyes-Iturbide J., Rosado M., Velázquez P. F., 2008, AJ, 136, 2011

Ridley J. P., Crawford F., Lorimer D. R., Bailey S. R., Madden J. H., Anella R., Chennamangalam J., 2013, MNRAS, 433, 138

Ridolfi A. et al., 2021, MNRAS, 504, 1407

Ridolfi A. et al., 2022, A&A, 664, A27

Robitaille T., Bressert E., 2012, APLpy: Astronomical Plotting Library in Python. Astrophysics Source Code Library, record ascl:1208.017

Rosado M., Laval A., Le Coarer E., Boulesteix J., Georgelin Y. P., Marcelin M., 1993, A&A, 272, 541

Sasaki M. et al., 2022, A&A, 661, A37

Scargle J. D., 1969, ApJ, 156, 401

Seward F. D., Harnden F. R. J., Helfand D. J., 1984, apjl, 287, L19

Stappers B., Kramer M., 2016, MeerKAT Science: On the Pathway to the SKA. p. 9

Staveley-Smith L. et al., 1996, PASA, 13, 243

Tauris T. M., van den Heuvel E. P. J., 2006, in Lewin W., van der Klis M., eds, Compact stellar X-ray sources, No. 39. Cambridge Univ. Press, p. 623

van Heerden E., Karastergiou A., Roberts S. J., 2017, MNRAS, 467, 1661

van Straten W., Demorest P., Oslowski S., 2012, Astron. Res. Technol., 9, 237

van den Eijnden J., Rajwade K., 2024, Res. Notes Am. Astron. Soc., 8, 34

Verbunt F., Igoshev A., Cator E., 2017, A&A, 608, A57

Wang Q. D., Gotthelf E. V., Chu Y. H., Dickel J. R., 2001, ApJ, 559, 275

Wang Y. et al., 2022, ApJ, 930, 38

Weltevrede P., 2016, A&A, 590, A109

Wenger M. et al., 2000, A&AS, 143, 9

Williams R. M., Chu Y. H., Dickel J. R., Gruendl R. A., Seward F. D., Guerrero M. A., Hobbs G., 2005, ApJ, 628, 704

Xie Y.-W. et al., 2019, Res. Astron. Astrophys., 19,103

Xu H. et al., 2023, Res. Astron. Astrophys., 23, 075024

Yao J. M., Manchester R. N., Wang N., 2017, ApJ, 835, 29

Yew M. et al., 2021, MNRAS, 500, 2336

Zanardo G., Staveley-Smith L., Gaensler B. M., Indebetouw R., Ng C. Y., Matsuura M., Tzioumis A. K., 2018, ApJ, 861, L9

Zangrandi F. et al., 2024, preprint (arXiv:2401.17307)

Zhang S. B., Dai S., Hobbs G., Staveley-Smith L., Manchester R. N., Russell C. J., Zanardo G., Wu X. F., 2018, MNRAS, 479, 1836

Zheng H. et al., 2017, MNRAS, 464, 3486

Zhu W. W. et al., 2014, ApJ, 781, 117

This paper has been typeset from a TEX/LATEX file prepared by the author.